Analog Studies of Upstream-Inclined Waves in Magnetogasdynamic Flow

LAWRENCE S. IWAN*
Cornell University, Ithaca, N. Y.

An analog has been devised to study two-dimensional magnetogasdynamic (MGD) flow for the case of aligned magnetic and velocity fields and a perfectly conducting compressible fluid. The analog consists of stretched elastic sheets in an incompressible fluid. The elastic sheets are analogous to a magnetic field and produce a body force on the fluid when displaced from their equilibrium positions. The differential equations describing the system are nearly the same as the MGD equations for the case cited, except for the expression for the body force in the momentum equations. Despite these differences, the small disturbance propagation characteristics of the analog system are strikingly similar to those of MGD. In particular, it is shown that it is possible to simulate the conditions under which forward-inclined disturbance waves are predicted in MGD flows about bodies. An experiment was performed in which a body was towed along a tank filled with water in which sheets of natural rubber had been stretched to simulate a uniform magnetic field. Upstream-inclined waves whose angles with the direction of the body's motion agreed well with the predicted values were observed.

I. Introduction

ONE of the most interesting features that arises in the study of MGD flow past bodies is the prediction of wave- and wake-like disturbances that propagate upstream ahead of the body. There has been considerable discussion and some dispute over the nature of these disturbances. Some authors[2-4] feel that the disturbances are similar in form to the waves and wakes of ordinary fluid dynamics, whereas others[5] feel that the form of the disturbances is more restricted.

In order to cast some light on the analytical results that have been presented to date, it is necessary to perform some experiments in the laboratory under conditions that permit the observation of the flow patterns around bodies. However, it is difficult to create conditions in the laboratory under which the forward-propagating disturbances could be observed, because the high fluid conductivity and strong magnetic fields required are difficult to create and maintain.

This paper describes the study of an analog to two-dimensional MGD flow that exhibits the forward-facing wave phenomenon. Stretched rubber sheets are used to represent a magnetic field, and water is used to represent the fluid. This analog, "elastohydrodynamics" (EHD), is not described by precisely the same differential equations as MGD, but the essential features that give rise to forward-propagating disturbances are present in both cases. The existence and nature of the forward waves in the EHD case may yield some information about corresponding phenomena in MGD.

II. Discussion of the Analog

A. Derivation of the Basic Equation

The derivation of the EHD fluid-flow equations is based on the model described below and is illustrated in Fig. 1. A two-dimensional array of elastic sheets exists in an incompressible fluid of density ρ. The sheets are infinitesimally thick and arbitrarily closely spaced. Each sheet is subject to tension T per unit width. The stresses as well as the normals to the sheet surfaces lie in the x-y plane and are functions of x, y, and time t, only. This is a case of plane stress. The fluid slips freely along the sheets, but no fluid may flow across a sheet. When there is no flow, the sheets are parallel to the x-y plane and uniformly spaced.

We introduce an elastic "stream function," $F(x, y, t)$ that is constant on any given sheet and that changes its value by unity as we move from the given sheet to an adjacent sheet. Thus, $1/F_x \equiv (\partial F/\partial x)^{-1}$ and $1/F_y \equiv (\partial F/\partial y)^{-1}$ represent the distance between adjacent sheets in the x and y directions, respectively. $1/F_n \equiv (F_x^2 + F_y^2)^{-1/2} \equiv \delta$ is the normal distance between adjacent sheets.

To identify the stretched elastic sheets with a two-dimensional magnetic field $\mathcal{H}$, we note that $F\mathbf{k}$ (where $\mathbf{k}$ is a unit vector in the z direction) corresponds to the vector potential of plane electromagnetics. Thus $\mathcal{H} = \nabla \times F\mathbf{k} = F_y\mathbf{i} - F_x\mathbf{j}$ (where $\mathbf{i}$ and $\mathbf{j}$ are unit vectors in the x and y directions, respectively) is a vector that is tangent to the sheet surface and whose length is inversely proportional to δ, the normal distance between sheets. The condition div $\mathcal{H} = 0$ is automatically satisfied.

The momentum equations can be written if we know the body force due to the displacement of the sheets from their equilibrium position. Consider the segment ΔS of the sheet of Fig. 2. The x component of force per unit depth due to the curvature of the segment is

$$\Delta X = T(\cos\theta_2 - \cos\theta_1) \cong Td/ds(\cos\theta)\,\Delta S \qquad (1)$$

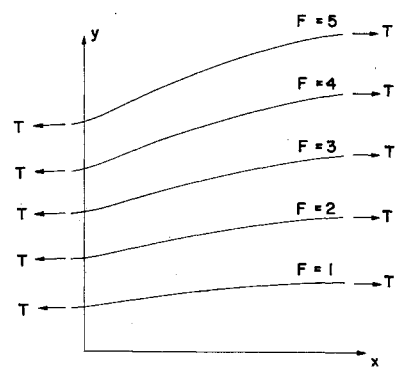

Fig. 1 Model for EHD.

Received August 24, 1964; revision received December 3, 1964. This research was supported in part by the Air Force Office of Scientific Research Grant No. AF-AFOSR-62-201. The author is indebted to William R. Sears for his helpful advice, his encouragement, and his enduring interest throughout the course of this study.

* Graduate Student, Graduate School of Aerospace Engineering. Student Member AIAA.

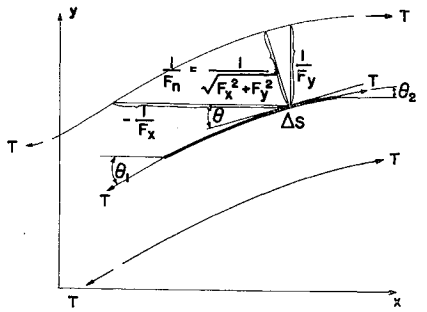

Fig. 2 Sketch showing quantities mentioned in the derivation of EHD body force.

where d/ds is the derivative along the sheet

$$d/ds(\cos\theta) = (\cos\theta\partial/\partial x + \sin\theta\partial/\partial y)(\cos\theta) \tag{2}$$

Now

$$\cos\theta = F_y/F_n \qquad \text{and} \qquad \sin\theta = -F_x/F_n \tag{3}$$

Thus

$$\Delta X = (T\Delta S/F_n{}^4)(2F_x{}^2F_yF_{xy} - F_xF_y{}^2F_{xx} - F_x{}^3F_{yy}) \tag{4}$$

This force acts on the area $\Delta S\delta = \Delta S/F_n$ and the force per unit volume X is obtained by dividing ΔX the force per unit depth by the area on which it acts:

$$X = \Delta X/\Delta S\delta = (T/F_n{}^3)(2F_x{}^2F_yF_{xy} - F_xF_y{}^2F_{xx} - F_x{}^3F_{yy}) \tag{5}$$

Similarly, the y component of the body force is

$$Y = (T/F_n{}^3)(2F_xF_y{}^2F_{xy} - F_y{}^3F_{xx} - F_x{}^2F_yF_{yy}) \tag{6}$$

So the momentum equations can then be written as

$$\rho Du/Dt = -\partial p/\partial x + X \tag{7}$$

$$\rho Dv/Dt = -\partial p/\partial y + Y \tag{8}$$

where D/Dt is the convective derivative $\partial/\partial t + u(\partial/\partial x) + v(\partial/\partial y)$, p is the pressure, u and v are the x and y velocity components, respectively.

The condition that no fluid flows through a sheet is analogous to Ohm's law in MGD when the fluid conductivity is infinite. This law states that fluid particles must always move on the same magnetic field lines. This condition can be expressed by a single differential equation:

$$DF/Dt = 0 \tag{9}$$

The convective derivative D/Dt denotes differentiation following the motion of a fluid particle, and so the expression (9) states that a fluid particle moves on a line of constant F. But F = const is merely the equation describing the surface of an elastic sheet, and so (9) does state that fluid particles must follow the "field lines."

The continuity equation is unaffected by the presence of the elastic sheets and is given by

$$\partial\rho/\partial t + \nabla\cdot(\rho\mathbf{q}) = 0 \tag{10a}$$

where ρ is the fluid density and $\mathbf{q}$ is the fluid velocity; or, where the fluid is incompressible,

$$\nabla\cdot\mathbf{q} = \partial u/\partial x + \partial v/\partial y = 0 \tag{10b}$$

B. Comparison of EHD with MGD

MGD is described by a set of equations that is quite similar to those derived previously for EHD. There is a body-force term in the momentum equation $\mathcal{J} \times \mathbf{B}$ which gives the force on the fluid due to the interaction of electric current $\mathcal{J}$ with the magnetic field $\mathbf{B}$. We express $\mathcal{J}$ in terms of $\mathbf{B}$

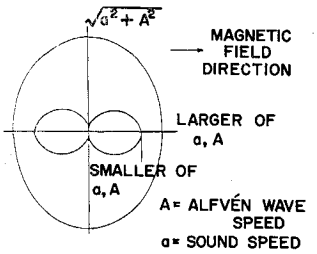

Fig. 3 Hodograph of propagation velocities of plane MGD waves.

by means of one of Maxwell's equations and substitute in the body-force expression to find

$$\mathcal{J} \times \mathbf{B} = (\mu^{-1}\nabla \times \mathbf{B}) \times \mathbf{B} = \mu(\nabla \times \mathbf{H}) \times \mathbf{H} \tag{11}$$

which is, in two dimensions,

$$\mathcal{J} \times \mathbf{B} = \mathbf{i}\mu H_{(y)}(\partial H_{(x)}/\partial y - \partial H_{(y)}/\partial x) + \mathbf{j}\mu H_{(x)}(\partial H_{(y)}/\partial x - \partial H_{(x)}/\partial y) \tag{12}$$

where the subscripts in parentheses indicate vector components.

Ohm's law describes the coupling between the magnetic field and flow field. Ohm's law is

$$\mathcal{J} = \sigma(\mathbf{E} + \mathbf{q} \times \mathbf{B}) \tag{13}$$

where σ is the fluid conductivity, and $\mathbf{E}$ is the electric field. When $\sigma \to \infty$, infinite currents may be avoided only if

$$\mathbf{E} + \mathbf{q} \times \mathbf{B} = 0 \tag{14}$$

Take the curl of this equation and get

$$\nabla \times \mathbf{E} + \nabla \times (\mathbf{q} \times \mathbf{B}) = 0 \tag{15}$$

Make use of another of Maxwell's equations

$$\nabla \times \mathbf{E} = -\partial\mathbf{B}/\partial t$$

and find

$$\left.\begin{aligned} &\partial\mathbf{B}/\partial t + \mathbf{B}(\nabla\cdot\mathbf{q}) - \mathbf{q}(\nabla\cdot\mathbf{B}) + (\mathbf{q}\cdot\nabla)\mathbf{B} - (\mathbf{B}\cdot\nabla)\mathbf{q} = 0 \\ \text{or} \\ &\partial\mathbf{H}/\partial t + \mathbf{H}(\nabla\cdot\mathbf{q}) - \mathbf{q}(\nabla\cdot\mathbf{H}) + (\mathbf{q}\cdot\nabla)\mathbf{H} - (\mathbf{H}\cdot\nabla)\mathbf{q} = 0 \end{aligned}\right\} \tag{16}$$

Noting that $(\nabla\cdot\mathbf{H}) = 0$ and writing the components of (16) for the two-dimensional case, we get

$$\frac{\partial H_{(x)}}{\partial t} + u\frac{\partial H_{(x)}}{\partial x} + v\frac{\partial H_{(x)}}{\partial y} + H_{(x)}\frac{\partial v}{\partial y} - H_{(y)}\frac{\partial u}{\partial y} = 0$$

$$\frac{\partial H_{(y)}}{\partial t} + u\frac{\partial H_{(y)}}{\partial x} + v\frac{\partial H_{(y)}}{\partial y} + H_{(y)}\frac{\partial u}{\partial x} - H_{(x)}\frac{\partial v}{\partial x} = 0 \tag{17}$$

In the two-dimensional case, (17) holds for both compressible and incompressible flows.

In order to facilitate the comparison of the EHD and MGD equations, we note that the analog field was written as

$$\mathcal{K} = F_y\mathbf{i} - F_x\mathbf{j} = \mathcal{K}_{(x)}\mathbf{i} + \mathcal{K}_{(y)}\mathbf{j} \tag{18}$$

and substitute $\mathcal{K}_{(x)}$ for F_y and $\mathcal{K}_{(y)}$ for $-F_x$ in the EHD equa-

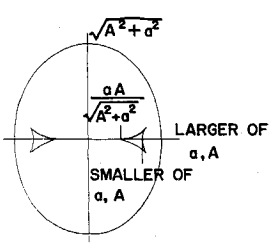

Fig. 4 MGD Friedrichs diagram.

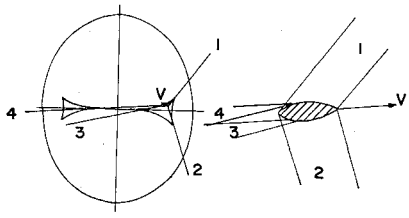

Fig. 5 Determination of the steady flow wave pattern by means of a construction on the Friedrichs diagram.

tions. We then write the EHD and MGD equations in corresponding pairs. The expression (9) must be differentiated with respect to y to compare it with the x component of Ohm's law, and with respect to x to compare it with the y component of Ohm's law.

x Momentum

$$\text{EHD}\quad \frac{Du}{Dt} = -\frac{1}{\rho}\frac{\partial p}{\partial x} + \left(\frac{T}{\rho\mathcal{H}^3}\right)\times \left(2\mathcal{H}_{(y)}{}^2\mathcal{H}_{(x)}\frac{\partial\mathcal{H}_{(x)}}{\partial x} - \mathcal{H}_{(y)}\mathcal{H}_{(x)}{}^2\frac{\partial\mathcal{H}_{(y)}}{\partial x} + \mathcal{H}_{(y)}{}^3\frac{\partial\mathcal{H}_{(x)}}{\partial y}\right) \quad (19)$$

$$\text{MGD}\quad \frac{Du}{Dt} = -\frac{1}{\rho}\frac{\partial p}{\partial x} + \frac{\mu}{\rho}H_{(y)}\left(\frac{\partial H_{(x)}}{\partial y} - \frac{\partial H_{(y)}}{\partial x}\right) \quad (20)$$

y Momentum

$$\text{EHD}\quad \frac{Dv}{Dt} = -\frac{1}{\rho}\frac{\partial p}{\partial y} + \left(\frac{T}{\rho\mathcal{H}^3}\right)\times \left(2\mathcal{H}_{(y)}\mathcal{H}_{(x)}{}^2\frac{\partial\mathcal{H}_{(y)}}{\partial y} + \mathcal{H}_{(x)}{}^3\frac{\partial\mathcal{H}_{(y)}}{\partial x} - \mathcal{H}_{(y)}{}^2\mathcal{H}_{(x)}\frac{\partial\mathcal{H}_{(x)}}{\partial y}\right) \quad (21)$$

$$\text{MGD}\quad \frac{Dv}{Dt} = -\frac{1}{\rho}\frac{\partial p}{\partial y} + \frac{\mu}{\rho}H_{(x)}\left(\frac{\partial H_{(y)}}{\partial x} - \frac{\partial H_{(x)}}{\partial y}\right) \quad (22)$$

x Component of Ohm's Law

$$\text{EHD}\quad \frac{\partial\mathcal{H}_{(x)}}{\partial t} - \mathcal{H}_{(y)}\frac{\partial u}{\partial y} + \mathcal{H}_{(x)}\frac{\partial v}{\partial y} + u\frac{\partial\mathcal{H}_{(x)}}{\partial x} + v\frac{\partial\mathcal{H}_{(x)}}{\partial y} = 0 \quad (23)$$

$$\text{MGD}\quad \frac{\partial H_{(x)}}{\partial t} - H_{(y)}\frac{\partial u}{\partial y} + H_{(x)}\frac{\partial v}{\partial y} + u\frac{\partial H_{(x)}}{\partial x} + v\frac{\partial H_{(x)}}{\partial y} = 0 \quad (24)$$

y Component of Ohm's Law

$$\text{EHD}\quad \frac{\partial\mathcal{H}_{(y)}}{\partial t} + \mathcal{H}_{(y)}\frac{\partial u}{\partial x} - \mathcal{H}_{(x)}\frac{\partial v}{\partial x} + u\frac{\partial\mathcal{H}_{(y)}}{\partial x} + v\frac{\partial\mathcal{H}_{(y)}}{\partial y} = 0 \quad (25)$$

$$\text{MGD}\quad \frac{\partial H_{(y)}}{\partial t} + H_{(y)}\frac{\partial u}{\partial x} - H_{(x)}\frac{\partial v}{\partial x} + u\frac{\partial H_{(y)}}{\partial x} + v\frac{\partial H_{(y)}}{\partial y} = 0 \quad (26)$$

The continuity equation is the same in both cases:

$$\partial\rho/\partial t + \nabla\cdot(\rho\mathbf{q}) = 0 \quad (27)$$

or $\nabla\cdot\mathbf{q} = 0$ when the flow is incompressible.

The analog is not described by the differential equations for MGD, but the difference between the two sets of equations is only in the body-force terms in the momentum equations. The body force is perpendicular to the field lines in both cases, but the magnitude of the force is given by different expressions. As we shall see, we will still be able to simulate some of the MGD flow phenomena that we set out to investigate.

In discussing sub- and super-Alfvénic flows past bodies in MGD, it is helpful to consider the hodograph of the propagation velocities of magnetoacoustic plane waves and the "Friedrichs diagram," that is derived from the propagation-velocity hodograph.[3] When the fluid is compressible, the wave-velocity hodograph has the appearance of Fig. 3 for two-dimensional and axisymmetric flows.

Figure 4, the Friedrichs diagram, is derived from Fig. 3 by constructing the envelope of normals to the wave vectors of Fig. 3. It represents the ultimate shape of a disturbance wave that propagates from a point disturbance at the origin.

To find the inclination of waves in the flow about a slender body or far from an arbitrary body, one draws the velocity vector on the Friedrichs diagram and draws all possible tangents from the tip of the vector to the pulse curves. The tangents to the pulse curves have the same inclinations to the field direction as the waves. When a body's velocity vector lies inside one of the cusped triangles of the Friedrichs diagram, there are forward-inclined waves. Figure 5 shows such a construction on the Friedrichs diagram and the resultant wave pattern in the fluid through which the body is moving at the specified velocity.

For the velocity depicted in Fig. 5, there are four families of waves as shown, all inclined at different angles with respect to the velocity vector. For "aligned-fields" flow, when the velocity vector lies in the direction of the applied magnetic field, the two families of forward-inclined waves make equal angles with the velocity vector, and the two rearward-inclined families collapse into a single family parallel to the velocity vector.

Figure 6, the "Taniuti-Resler" diagram, shows the various flow regimes for aligned-fields compressible flow. In each area of the diagram there is a sketch of the characterizing features of flow around a body whose velocity falls in that regime. Forward propagating disturbances occur for $0 < m < 1, 0 < M < 1$. The disturbance is wake-like for $m^2 + M^2 < 1$ and wave-like for $m^2 + M^2 > 1$.

Similar diagrams may be drawn for EHD flow. We must first find the wave-velocity hodograph and from it construct

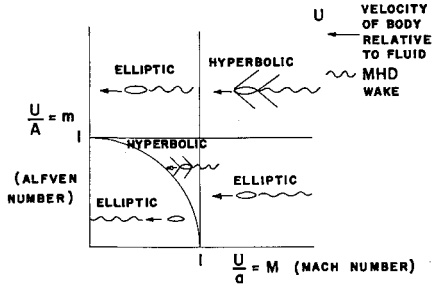

Fig. 6 Taniuti-Resler diagram for aligned-fields compressible MGD.

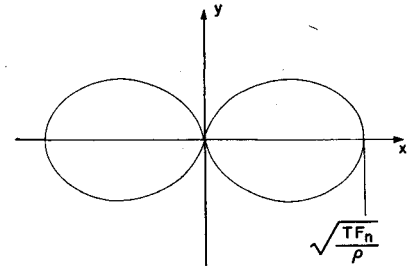

Fig. 7 Hodograph of propagation velocities of plane EHD waves.

an appropriate Friedrichs diagram. We follow the methods used by Friedrichs and Kranzer for MGD waves.[1]

Small disturbances will propagate on the characteristic surfaces, so let us find the characteristic surface propagation velocities. Let $\pm c$ be the characteristic velocity relative to the fluid, and choose coordinates so that c is in the x direction. To find the changes across a characteristic, write the differential equations for EHD when the fluid is incompressible in the following way:

$$\rho[u_t + (u \pm c)u_x \pm cu_x + vu_y] = -p_x + (T/F_n^3)(2F_x^2F_yF_{xy} - F_xF_y^2F_{xx} - F_x^3F_{yy}) \quad (28)$$

$$\rho[v_t + (u \pm c)v_x \mp cv_x + vv_y] = -p_y + (T/F_n^3)(2F_xF_y^2F_{xy} - F_y^3F_{xx} - F_x^2F_yF_{yy}) \quad (29)$$

$$u_x + v_y = 0 \quad (30)$$

$$F_{yt} + F_xu_y + F_yv_y + (u \pm c)F_{yx} \mp cF_{yx} + vF_{yy} = 0 \quad (31)$$

$$F_{xt} + F_xu_x + F_yv_x + (u \pm c)F_{xx} \mp cF_{xx} + vF_{xy} = 0 \quad (32)$$

Since $u \pm c$ is the velocity of the characteristic surface, $R_t + (u \pm c)R_x$ is the time derivative of the quantity R at a point that moves with the velocity of the characteristic surface. Such a derivative must be continuous since the point does not cross the characteristic surface. Likewise, all y derivatives are continuous, because the y direction is parallel to the characteristic surface. The derivatives can be discontinuous across the characteristic surface; however, so integrating Eqs. (28–32) to find the change across the characteristic surface, we get

$$\mp \rho c\delta u = -\delta p - (T/F_n^3)(F_xF_y^2\delta F_x - 2F_x^2F_y\delta F_y) \quad (33)$$

$$\mp \rho c\delta v = -(T/F_n^3)(F_y^3\delta F_x - 2F_xF_y^2\delta F_y) \quad (34)$$

$$\delta u = 0 \quad (35)$$

$$\mp c\delta F_y = 0 \quad (36)$$

$$F_x\delta u \mp c\delta F_x + F_y\delta v = 0 \quad (37)$$

where δR is the jump of the quantity R across a characteristic. Equations (35) and (36) allow us to simplify (33, 34, and 37), giving us the following equations:

$$\delta p + (T/F_n^3)F_xF_y^2\delta F_x = 0 \quad (38)$$

$$\mp\rho c\delta v + (T/F_n^3)F_y^3\delta F_x = 0 \quad (39)$$

$$\mp c\delta F_x + F_y\delta v = 0 \quad (40)$$

If the solution to the set of equations (38–40) is to be nontrivial, the determinant of the coefficients of the quantities $\delta p, \delta F_x, \delta v$ must be zero, i.e.,

$$\begin{vmatrix} 1 & 0 & (T/F_n^3)F_xF_y^2 \\ 0 & \mp\rho c & (T/F_n^3)F_y^3 \\ 0 & F_y & \mp C \end{vmatrix} \quad (41)$$

or

$$\rho c^2 - TF_y^4/F_n^3 = 0 \quad (42)$$

Let θ be the angle between the y axis and the normal to the surface of the elastic sheets. Then

$$F_y = F_n\cos\theta$$

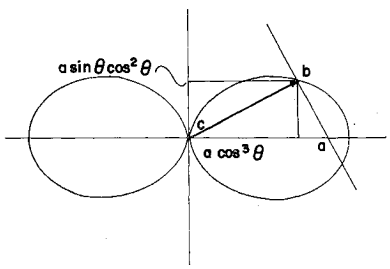

Fig. 8 Construction of EHD Friedrichs diagram from wave velocity hodograph.

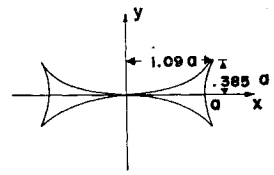

Fig. 9 Friedrichs diagram for EHD.

and

$$C = (TF_n/\rho)^{1/2}\cos^2\theta \quad (43)$$

The hodograph of the wave velocities is shown in Fig. 7. Thus, for EHD, there is only one set of waves, those that correspond to the "slow waves" of MGD.

The Friedrichs diagram is easy to construct either graphically or analytically from the velocity hodograph. As stated previously, it is the envelope of the normals to the wave velocity vectors. One point on the envelope is the intersection of the normal to one wave velocity vector inclined at an angle θ to the x axis, with the normal to another vector inclined at $\theta + d\theta$ to the x axis, where $d\theta$ is infinitesimal. If such a point can be found for every value of θ, then the Friedrichs diagram is the locus of all such points.

To construct a point on the envelope, proceed in the following manner: 1) construct the normal to one wave vector in the hodograph plane passing through the tip of the vector, and 2) construct a similar normal for a second wave vector inclined at a very small angle $d\theta$ to the first vector. The intersection of the two vector normals in the limit as $d\theta \to 0$ is one point of the Friedrichs diagram. We find the Friedrichs diagram curves analytically, following the preceding procedure. The wave velocity hodograph is represented in polar coordinates by the equation

$$r = \mathfrak{A}\cos^2\theta \quad (44)$$

where

$$\mathfrak{A} = (TF_n/\rho)^{1/2}$$

and θ is the inclination of the wave-velocity vector to the x axis. Then the Cartesian components of the wave velocity are

$$\left.\begin{aligned} x &= \mathfrak{A}\cos^3\theta \\ y &= \mathfrak{A}\sin\theta\cos^2\theta \end{aligned}\right\} \quad (45)$$

Referring to Fig. 8, the normal to bc that passes through b is given by the equation

$$y = \cot\theta(\mathfrak{A}\cos\theta - x) \quad (46)$$

In order to find the intersection (x_i, y_i) of the normals to two different wave vectors, set $y_{i1} = y_{i2} = y_i$ and get

$$y_i = \cot\theta_1(\mathfrak{A}\cos\theta_1 - x_{i1}) = \cot\theta_2(\mathfrak{A}\cos\theta_2 - x_{i2}) \quad (47)$$

but

$$x_{i1} = x_{i2} = x_i = \frac{\mathfrak{A}(\cot\theta_2\cos\theta_2 - \cot\theta_1\cos\theta_1)}{\cot\theta_2 - \cot\theta_1} \quad (48)$$

Let $\theta_2 = \theta_1 + \delta = \theta + \delta$ and then let $\delta \to 0$ to obtain

$$\left.\begin{aligned} x_i &= \mathfrak{A}\cos\theta(1 + \sin^2\theta) \\ y_i &= -\mathfrak{A}\cos^2\theta\sin\theta \end{aligned}\right\} \quad (49)$$

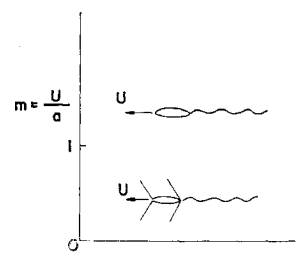

Fig. 10 Resler-Taniuti diagram for aligned-fields EHD.

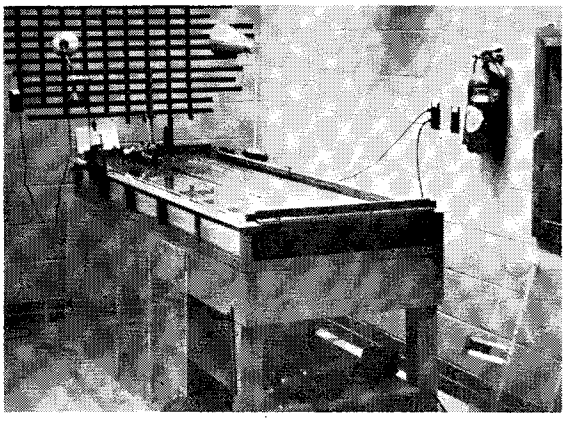

Fig. 11 View of the apparatus in the laboratory.

These are the parametric equations for the Friedrichs pulse curve, which is shown in Fig. 9. The disturbance pulse consists of a pair of cusped triangles that meet at the origin and extend along the "field" direction as shown. A body moving in the x direction with velocity U will produce forward-inclined waves when $|U| < \mathfrak{A}$ and trailing wakes when $|U| > \mathfrak{A}$. The wave inclination is found with the aid of the EHD Friedrichs diagram in the same way that the wave inclination for MGD flow is found with the MGD Friedrichs diagram.

The Taniuti-Resler diagram for aligned fields EHD flow (Fig. 10) is very simple. Since the fluid is incompressible, the Mach number M is always zero. There are only two flow regimes: an elliptic regime with downstream wakes for $m = U/\mathfrak{A} > 1$, and a hyperbolic regime with upstream-inclined waves for $m < 1$. It should be emphasized that this is different from the case $M \to 0$ in MGD. When the fluid is incompressible in MGD, there are two elliptic regimes which differ from one another in that the wake lies upstream for sub-Alfvénic flows and downstream for super-Alfvénic flows.

The sub-Alfvénic regime in EHD, then, is analogous to the sub-Alfvénic, subsonic hyperbolic regime in magnetogasdynamics. Because the cusped triangles in the EHD diagram meet at the origin, there is no sub-Alfvénic elliptic regime, and only upstream-inclined waves may be observed. Upstream wakes do not occur.

III. Description of the Experiment

A. Apparatus

The experiment was conducted in a glass tank 90 in. long and 30 in. wide, filled with water to a depth of 4.5 in. The tank and its frame of angle iron were supported on a wooden table. For part of the experiment a lucite cover rested on the surface of the water. The cover was supported by 4.5-in. supports inside the tank along its sides. Twenty-eight thin

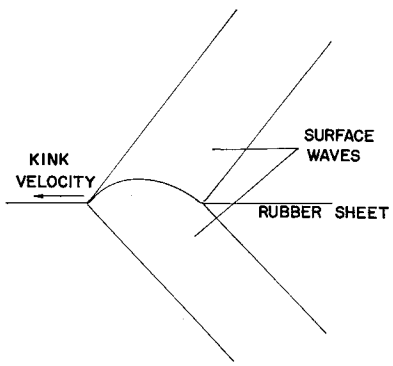

Fig. 12 Surface waves produced by a traveling disturbance.

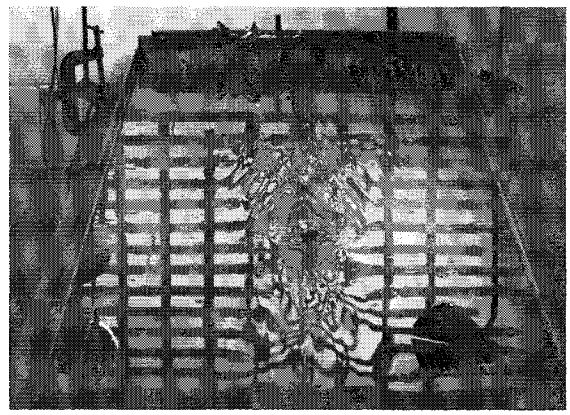

Fig. 13a Disturbance pattern produced by impulsive motion of a piston.

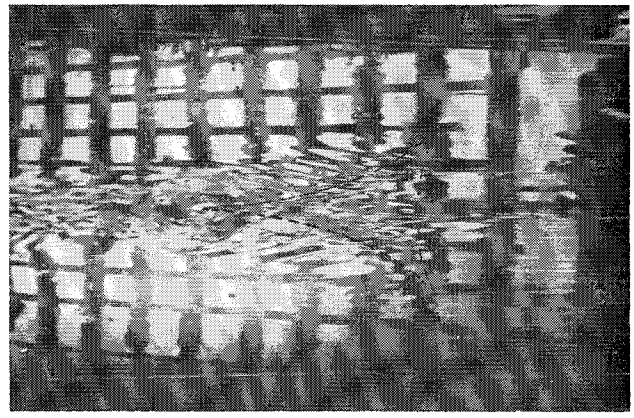

Fig. 13b Disturbance pattern produced by impulsive motion of a piston; corrected perspective.

sheets of natural rubber were stretched lengthwise inside the tank and anchored at the ends of the tank in brackets 1 in. apart. Natural rubber was chosen because of its impermeability to water and its elastic properties. The sheets were stretched to about one and one-half times their unstressed length, so that small deflections of the sheets from their equilibrium position did not change the tension by an appreciable fraction. Each sheet was stretched to a tension per unit width of 8.5 lb/ft giving a calculated wave speed in the field direction of 7.2 fps. Figure 11 is a photograph of the tank in the laboratory. The tank has been filled with water, and the rubber sheets have been stretched and anchored in the tank and are visible in the photograph. The lucite cover is leaning against the side of the table.

Disturbances were visible as traveling two-dimensional kinks in the rubber sheets. A plane wave front moving down the tank could be created by striking the tank sharply on one side near the end. The speed of the wave front was determined from the time required for the front to travel from the support brackets at one end of the tank to those at the other end and return. The measured speed of the wave front was 7.5 ± 0.4 fps.

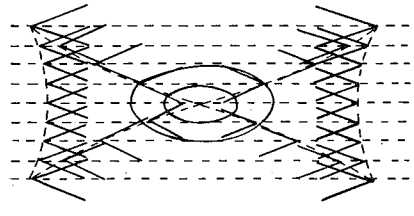

Fig. 14 Relationship of surface wave pattern to EHD disturbance pattern.

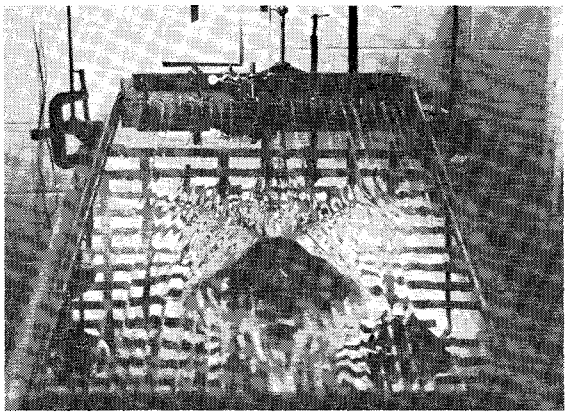

Fig. 15 Forward-inclined waves produced by a towed body; "Alfvén number" = 0.26. The motion is toward the far end of tank at top of photograph.

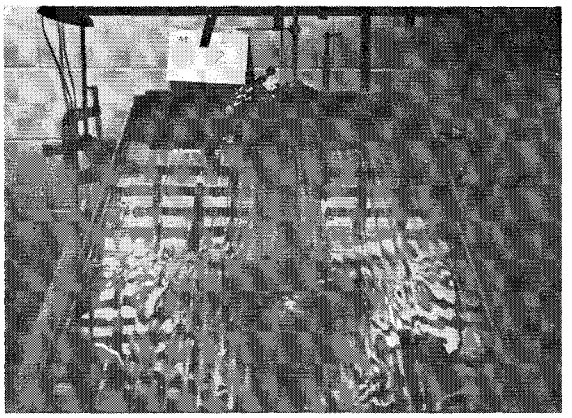

Fig. 16 Forward-inclined waves produced by a towed body; "Alfvén number" = 0.91.

Small disturbances were created by impulsive motion of a piston between one pair of rubber sheets in the tank. With the lucite cover on the tank, an observer could see the growing disturbance pattern shaped more or less like the cusped triangles of Fig. 9. But photographing the pattern was very difficult. The kinks in the sheets were very slight and visible to the eye, chiefly because they were moving. Several schemes were tried to make them visible in photographs, but only one was successful.

When the lucite cover was removed, the moving rubber sheets created surface waves that were quite visible in photographs. Each kink traveling down a sheet created a set of ordinary surface waves as illustrated in Fig. 12. The disturbance front could be found by tracing each set of surface waves to its source point and drawing a curve through all source points. In order to photograph the surface waves, the camera was placed so that it photographed the reflection in the tank of a grid on the laboratory wall. Surface waves distorted the reflection of the grid pattern revealing their structure. The grid on the wall is shown in the photograph of the apparatus.

B. Experimental Results

Figures 13a and 13b show the surface-wave pattern that results from a disturbance pulse created by the piston. Both figures come from the same negative, but the enlarger was tilted in printing Fig. 13b in order to correct the scale in the horizontal plane. The disturbance front is outlined on Fig. 13b.

The disturbance pattern is somewhat more complicated with the cover removed than it is with the cover in place. In addition to the wave pattern created by the kinks traveling along the sheets, there is a pattern of spreading ripples centered about the front edge of the piston. The ripple pattern is not circular, but is compressed in the direction normal to the rubber sheets. The ripples seem to propagate with the speed of "shallow water" gravity waves [$c_g = (gh)^{1/2} = 3.5$ fps for water 4.5-in. deep] along the tank and at a lower velocity across it. Thus, the disturbance pulse looks something like Fig. 14. The rubber sheets and the EHD disturbance front are drawn as dashed lines. At each point where the front intersects a rubber sheet is a moving kink that is the source of a set of waves.

The patterns in the photographs of Figs. 13a and 13b have the appearance of Fig. 14. The additional disturbance toward the far end of the tank in Figs. 13a and 13b is from the cord that was attached to the piston and was used to move it.

The pictures of forward-inclined waves are more easily interpreted. In order to produce forward-inclined waves, a body was towed in the tank at constant speed by means of a cord which was attached to the body and passed over several idler pulleys to a rotating shaft under the tank. A pulley on the shaft was driven by a belt from a pulley on a fractional horsepower electric motor to wind up the cord on the shaft, thereby towing the body. By varying the combination of motor and shaft pulleys, the shaft rpm could be varied to adjust the speed of the body as desired. The body, a lucite block with rounded corners, was $4\frac{1}{2}$ in. high, 8 in. long, and $1\frac{1}{2}$ in. thick. Upstream-inclined disturbance waves were observed when the body was towed at "sub-Alfvénic" speeds.

In Table 1, the experimental conditions for the towed-body flows are listed, and the predicted angles between the waves and the velocity vector are compared to the observed wave angles.

Figures 15 and 16 are two of the photographs from which the wave angles were determined. They were taken after the body had been towed part way down the tank and the

Table 1 Comparison of calculated and observed wave angles

Body speed, fps	Alfvén no.	Calculated wave angle	Observed wave angle
1.9	0.26	15°	16° ± 5°
2.16	0.30	18°	17° ± 4°
3.0	0.42	25°	25° ± 3°
3.75	0.52	32°	34° ± 3°
6.6	0.91	65°	58° ± 5°
7.5	1.04	No wave; flow is "super-Alfvénic"	No wave

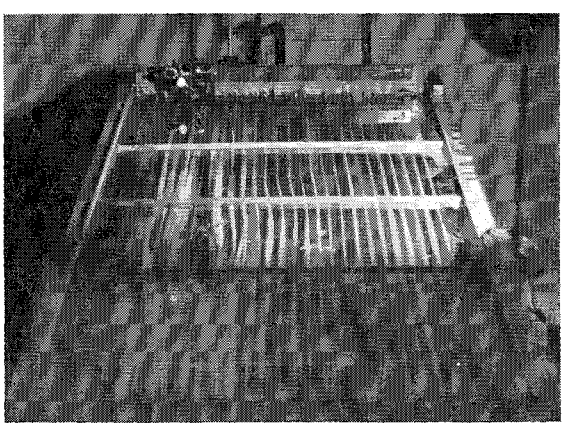

Fig. 17 Forward-inclined waves produced by a towed body; "Alfvén number" = 0.26; lucite cover on tank.

wave pattern had become fairly well developed. The body is moving toward the far end of the tank at the top of the photographs. Motion pictures were also made of the towed model flows at 64 frames/sec for Alfvén numbers of 0.26, 0.52, and 0.91; the wave angles were determined from measurements made on an optical comparator of a number of frames from each sequence.

Figure 17 is a photograph made with the cover on the tank. It shows quite clearly the deflection of the rubber sheets as the body is towed along the tank. The wave angles were determined with most certainty from the surface-wave measurements, however. Therefore Fig. 17 is included merely to show the two-dimensional disturbance waves in the tank.

C. Conclusions

Thus, we have observed forward-inclined disturbance waves, whose angles were predicted accurately by a method of analysis that parallels the analysis upon which the discussion of forward-inclined waves in MGD is based. We conclude that the picture of forward-facing waves and possibly upstream wakes, which has been presented in the literature, is probably correct.

The close agreement of the measured wave angles with their calculated values lends weight to the assertion that the EHD wave pattern is unaffected when the cover is removed from the tank in order to permit surface waves to reveal the EHD flow structure. Rigorous justification is possible if the wave-velocity analysis for the case of free surface EHD shows that there is no appreciable coupling between EHD waves and surface waves, but this has not been done at this time.

It might be possible to alter the model to include the study of finite electrical conductivity by perforating the elastic sheets. The size and density of holes would determine the rate of diffusion of the fluid across the field lines and hence the analog conductivity.

References

[1] Friedrichs, K. O. and Kranzer, H., "Notes on magnetohydrodynamics VIII. Nonlinear wave motion," Atomic Energy Commission Research and Development Rept., New York Univ. NYO-6486 (July 1958).

[2] Hasimoto, H., "Viscous flow of a perfectly conducting fluid with a frozen magnetic field," Phys. Fluids **2**, 337 (1959).

[3] Sears, W. R., "Some remarks about flow past bodies," Rev. Mod. Phys. **32**, 701–705 (1960).

[4] Sears, W. R. and Resler, E. L., Jr., "Sub- and super-Alfvénic flows past bodies," *Advances in Aeronautical Sciences* (Pergamon Press, Ltd., Oxford, England, 1961), Vols. 3 and 4, pp. 657–674.

[5] Stewartson, K., "On the motion of a non-conducting body through a perfectly conducting fluid," J. Fluid Mech. **8**, 82–96 (1960).

MAY 1965 AIAA JOURNAL VOL. 3, NO. 5

Evaluation of Electrode Shapes for Ion Engines

S. L. Eilenberg,* W. Seitz,† and E. Caplinger†
Electro-Optical Systems, Inc., Pasadena, Calif.

Techniques for evaluating electrode geometries for use in ion engines are presented. These techniques include the employment of a digital-computer program and an electrolytic tank. The study is separated into several problem areas, which include 1) direct interception, 2) charge-exchange interception, 3) uniformity of emission, and 4) beam collimation. Direct interception is discussed in terms of unsealed, sealed, and deactivated edges. The perimeter of the sastrugi geometry has been given special attention for focusing the outermost beams. Charge-exchange trajectories have been calculated. Because of the slope of field near the accel-aperture in an accel-decel system, the charge-exchange erosion pattern has features which distinguish it from direct interception. The consequences of this form of erosion are discussed. A possible solution to this problem is presented. The sastrugi geometry has some features that inherently produce nonuniform emission over part of its surface. The advantages and disadvantages of this characteristic are discussed, and electrolytic tank studies are described in which higher degrees of uniformity may be achieved if desired. In addition, digital-computer results are presented showing the wide variation of current densities over the sastrugi ionizer if full space-charge limited flow is achieved. The effect of the shape of the beam-plasma boundary on ion trajectories is also discussed.

Introduction

PRACTICAL ion engines for use on space missions must be designed to operate with long endurance capability. One of the most important areas to be considered in the design of such engines is that of electrostatic optics. It is necessary to determine the shape of electrodes which will produce the highest average current density and the lowest amount of particle interception on electrode surfaces. The need for a high average current density is dictated by the power efficiency requirement. This efficiency depends upon the ratio of the beam power emitted to the heat radiated per unit ionizer area. The higher this ratio, the more efficient the operation of the engine. It is also necessary to consider

Presented as Preprint 64-695 at the AIAA 4th Electric Propulsion Conference, Philadelphia, Pa., August 31–September 1, 1964; revision received December 15, 1964. This work was supported by the U. S. Air Force Aero Propulsion Laboratory Research and Technology Division, Wright-Patterson Air Force Base, Ohio, under Contract No. AF33(657)-10980. The authors express appreciation for the many helpful discussions with A. T. Forrester and T. Bates relating to the problems discussed in this paper, and the assistance of K. Carter and M. Hilbers in the reduction and analysis of data.

* Senior Scientist, Ion Physics Department. Member AIAA.
† Physicist.